ecdc
EUROPEAN CENTRE FOR DISEASE PREVENTION AND CONTROL

TECHNICAL REPORT

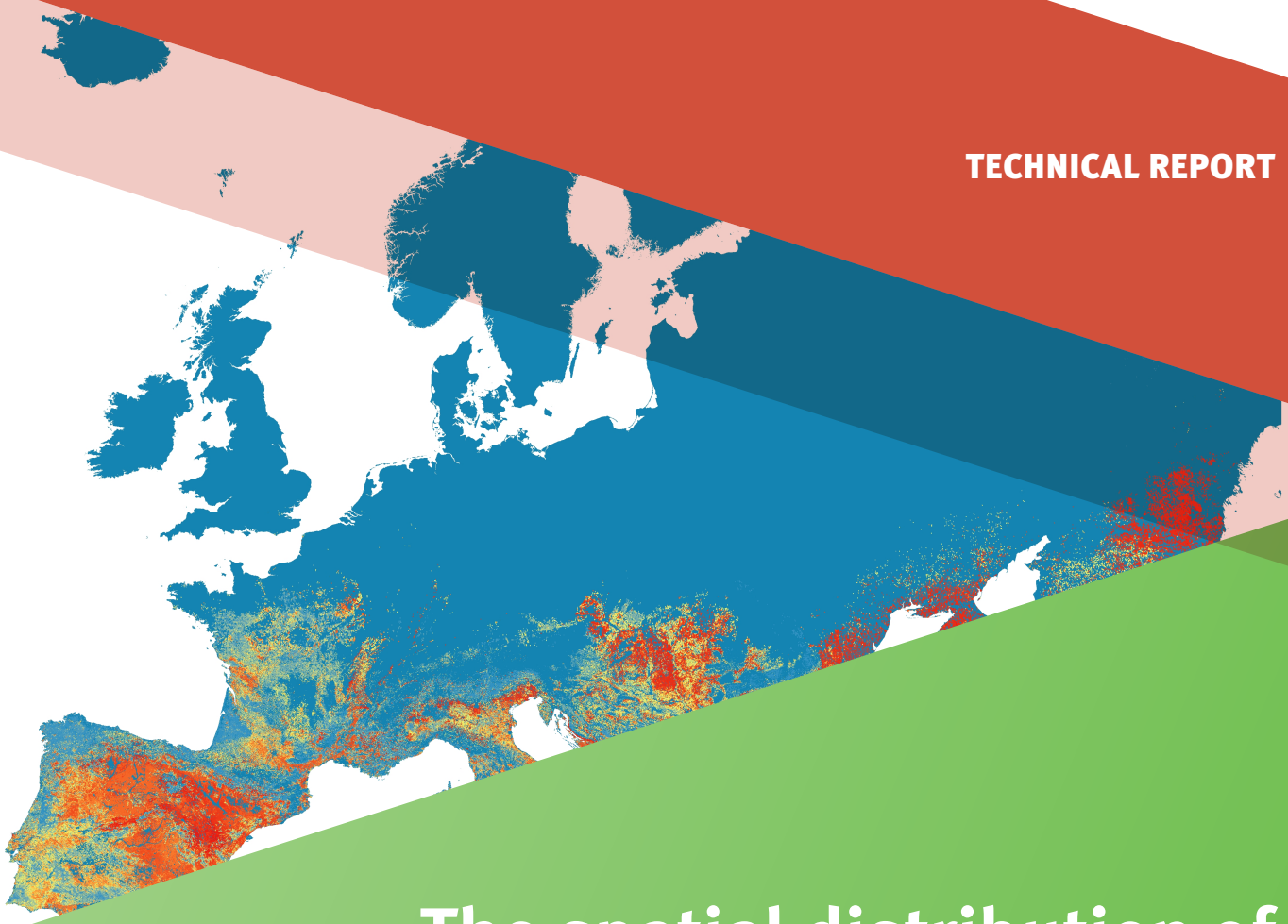

The spatial distribution of Crimean-Congo haemorrhagic fever in Europe and neighbouring areas

December 2023

ECDC TECHNICAL REPORT

The spatial distribution of Crimean-Congo haemorrhagic fever in Europe and neighbouring areas

December 2023

This report was commissioned by the European Centre for Disease Prevention and Control (ECDC) to assess the spatial distributions of Crimean-Congo haemorrhagic fever (CCHF) in Europe and neighbouring areas under specific contract No 4 ECD.13254 ID.13285 implementing inter-agency framework contract for services No ECDC/2019/020. The Horizon 2020 MOOD Project N° 874850 (https://https://mood-h2020.eu) provided the driver covariates and generated the vector distributions used in this report, which is catalogued by the project as MOOD0078. The contract was managed by Olivier Briet (ECDC).

Authors
Jane Messina, School of Geography and the Environment, and William Wint, Environmental Research Group, University of Oxford.

Acknowledgements
Thanks are due to Marieta Braks and Hein Sprong who managed the contract with ECDC, and Wim Van Bortel as VectorNet Scientific Support Work Package leader. These colleagues, together with Jolyon Medlock, Natalia Fernandez-Ruiz, Augustin Estrada-Pena, Kayleigh Hansford, Frank Sandmann, Sofie Dhollander, Céline Gossner, and Olivier Briet also provided invaluable guidance and comments on the technical report.

Suggested citation: European Centre for Disease Prevention and Control. The spatial distribution of Crimean-Congo haemorrhagic fever in Europe and its neighbours. Stockholm: ECDC; 2023.

Stockholm, December 2023

ISBN 978-92-9498-676-4
doi: 10.2900/222576
Catalogue number TQ-02-23-340-EN-N

Contents

Figures

Tables

Abbreviations

AIC	Akaike information criterion
BRT	Boosted Regression Trees
DEM	Digital Elevation Model
CCHF	Crimean-Congo haemorrhagic fever
CCHFV	Crimean-Congo haemorrhagic fever virus
ECMWF	European Centre for Medium-Term Weather Forecasting
EFSA	European Food Safety Authority
EU	European Union
EVI	Enhanced Vegetation Index
GBIF	Global Biodiversity Information Facility
GIS	Geographic Information System
LST	Land Surface Temperature
MODIS	Moderate Resolution Imaging Spectrometer
NASA	National Aeronautics and Space Administration
NDVI	Normalised Difference Vegetation Index
NUTS3	Nomenclature of Units for Territorial Statistics, level 3
RF	Random Forest

Executive summary

Crimean-Congo haemorrhagic fever (CCHF) is a tick-borne viral (*Nairovirus*, family Bunyaviridae) infection first identified in the Crimean region in 1944. It is one of the most widely distributed arboviral diseases in the world, ranging from southern Russia and the Black Sea region to the southern tip of Africa. The disease is considered as 'emerging' across the globe, with many countries reporting new CCHF cases in humans in recent decades, including Georgia, Türkiye, Albania and, most recently, Spain.

The distribution of CCHF was modelled globally in 2015 by Messina et al [1] and in 2020 by Okely et al [2] through ecological niche modelling, a technique which uses statistical correlations of presence and absence data with environmental variables such as temperature and landcover to spatially predict the ecological suitability (i.e. the probability of presence and absence) for the species or disease of interest in an area. Messina et al. predicted high probability areas for autochthonous disease to be in parts of eastern and southern Europe. It also predicted high ecological suitability for CCHF in areas of Spain, which was, however, hidden from view (masked) in the published distribution as the disease had then yet to be found in Iberia. The 2015 model also did not take into account the likely distributions of its main tick vectors in Europe, namely *Hyalomma marginatum* and *H. lusitanicum.* The Okely et al. study showed updated risk areas which included Spain, and also statistically compared the distribution of environments assessed as ecologically suitable for autochthonous acquisition of CCHF human disease to that of the primary tick vectors. Still, these vector distributions were not used to modify or mask (by hiding areas predicted to be environmentally suitable from view where the vectors are not present) the maps depicting environments assessed as ecologically suitable for autochthonous acquisition of human CCHF.

ECDC therefore asked that the 2015 modelled distributions of likely areas for autochthonous acquisition of CCHF for Europe and its neighbouring areas be re-estimated and updated, taking into account both the recent disease occurrence data and the distribution of its vectors. Two sets of spatial modelling were performed, both using a common covariate predictor data suite and long-established spatial modelling techniques. These models were a) for CCHF itself using Boosted Regression Trees (BRT), as used in 2015, and trained on presence data extracted from the published literature and statistically assigned pseudo-absence data, and b) for the two vector species using an ensemble of Random Forest and Boosted Regression Tree models, trained on presence data provided by the ECDC VectorNet project, other online databases and absence data based on calculated habitat suitability.

As the CCHF occurrence in Europe is too limited to establish reliable statistical correlations between CCHF presence and absence data in Europe and environmental covariates, the global distribution of the disease – including Europe, Africa, and Asia – was modelled, based on the assumption that a global model better informs a predicted distribution for Europe and its neighbouring areas.

The resulting model suggests substantially more areas with ecological suitability for autochthonous CCHF in Europe and its neighbouring areas than did the 2015 model, largely because more disease records were found in Albania, Greece, Spain, and Western Asia. The environmental suitability for autochthonous acquisition of the disease extends into much of northern Europe and the northern Caucasus – significantly beyond the vector distributions, which at worst restrict its northern range to about 49ºN (latitude of Paris, France).

The vector distribution models allow for refined mapping of areas of ecological suitability for autochthonous acquisition of CCHF compared to 2015 (where entire countries were masked out) by hiding (only) those areas in the basic CCHF spatial model from view (i.e. masking) where no vectors are present. When using the minimum predicted vector distribution as the mask, hiding a larger area with CCHF predicted suitability from view, much of the Mediterranean seaboard, the Balkans along with Türkiye and the Caucasus are predicted to be have patches suitable for CCHF. However, using the maximum predicted vector distribution as a mask, the resulting CCHF ecological suitability map matches the observed disease occurrences most closely, and on that map, the predicted suitability for CCHF extends significantly further north into parts of central France and eastward into central Europe.

This suggests that a number of countries that have yet to record CCHF may benefit from paying attention to this risk – especially those with Mediterranean coastlines. In comparison to the (masked) 2015 model, while much of Europe's ecological suitability for CCHF remains similar in this updated model, several subnational regions show increased ecological suitability for CCHF, particularly pockets throughout France, Italy, Spain, the Balkans, and the Caucasus.

Background

Crimean-Congo haemorrhagic fever (CCHF) is a tick-borne viral (Nairovirus, family Bunyaviridae) disease first identified in the Crimean region in 1944 [3,4]. It was subsequently shown to be the same virus as that causing similar haemorrhagic disease outbreaks in the Congo basin, giving the virus its current name [5,6]. CCHF is a widely distributed disease, ranging from eastern China to southern Russia and the Black Sea region, and to the southern tip of Africa [6].

The disease is considered as 'emerging' across the globe, with many countries reporting infections in humans in recent decades, including Albania (first occurrence in 2001) [7], Türkiye (in 2002) [8], Georgia (in 2009) [9], and Spain (in 2013) [10]. In some regions, human CCHF infection has also been recently reported after long periods of absence, for example in south-western Russia [11] and central Africa [12].

The disease is transmitted to humans by ticks, and while no apparent disease manifestation occurs in animals [13], both wild and domesticated animals represent an important link in the disease transmission cycle, acting as reservoirs for continued tick re-infection. Many tick species can carry CCHF virus (CCHFV), but members of the genus *Hyalomma* are considered the primary vectors and are the most common ticks known to transmit the virus to humans. In Europe, the relevant species are *Hyalomma marginatum* and *Hyalomma lusitanicum* [14]. These ticks are adapted to hot and dry or semiarid environments, and are found in many parts of Africa, Asia, and Europe [3,15–18]. Infection of humans is uncommon, although those living or working in close proximity to livestock are at greater at risk, and if infected then fatality can be as high as 40% [ref]. No CCHF-specific antiviral drug or vaccine currently exists for animals or humans.

The distribution of CCHF was modelled globally in 2015 by Messina *et al.* [1], a study which predicted autochthonous disease to be possible in parts of eastern and southern Europe. While the 2015 model successfully predicted that Spain was suitable for CCHF, the published outputs were adjusted so that ecological suitability for CCHF was only shown in countries that had reported cases. Spain was not shown as an area of ecological suitability in these outputs from the 2015 modelling, since the first case was (retroactively) reported in 2016 [19]. In addition, predictions of potential autochthonous CCHF distribution from other authors have become available [2]. The 2015 model also did not incorporate vector distributions in the disease predictions. Therefore, ECDC identified the need to update the earlier modelling exercise using up-to-date known distribution data to train (or calibrate) the model and including distributions for the two main European vectors (*H. marginatum* and *H. lusitanicum*) as additional disease model masks, to hide areas with predicted ecological CCHF suitability from view where the vectors are not present.

Methods

Overview

The modelling process involves establishing a statistical relationship between known presence (or absence) and the values of a series of selected predictor covariates. These relationships are calculated for a set of sample locations, and the estimated equations then applied to maps of the covariates which provide values at a pixel resolution for the entire area of interest. This results in a modelled spatial distribution showing the probability of presence at the resolution of the covariate maps – which were standardised in this project at 1 kilometre.

Two sets of spatial models were implemented for this study – one for CCHF in humans, and one for CCHF vectors, with the specific objective of providing predictions of areas ecologically suitable for autochthonous CCHF transmission to occur, for Europe and its neighbouring areas as far east as the Caspian Sea and to include northern Africa.

The distribution of the disease within Europe is somewhat restricted and the number of disease locations provides insufficient training data to run an effective model for the region. It was therefore necessary to run the disease model based on data from all countries globally to generate more robust estimates of the ecological correlates of autochthonous CCHF cases, which can then be applied to Europe to predict potential areas of ecological suitability in Europe.

While there are a number of different CCHF vector species within the global range of the disease, only two are widespread in Europe, namely *H. marginatum* which is found throughout southern Europe, the Middle East and northern Africa as far east as India; and *H. lusitanicum* which is limited to south-western Europe and neighbouring parts of northern Africa (e.g. Kolonin (2009) [20], Estrada-Pena *et al.* (2012),[21] VectorNet project [22]). The vectors were each modelled for their entire ranges plus a buffer zone (an area around the range boundary) of at least 200 km wide.

The methods used to generate vector and disease models were similar (see above) and the driver covariates offered to the models were drawn from the same standard covariate suite that has been used in modelling a range of vectors for ECDC and the European Food Safety Authority (EFSA) [23]. These covariates include indicators of level and seasonality

derived from MODIS satellite imagery time series using Temporal Fourier Analysis [24] for day and night land surface temperature (LST), vegetation indices, middle infrared and relative humidity; and for rainfall derived from the European Centre for medium Term Weather Forecasting (ECMWF) datasets. Consensus land use, as well as topographic and demographic variables were also part of the covariate suite. These are set out in detail in Supplementary Table 2 in the Annex. All datasets were standardised to ensure consistent spatial resolution and extent.

Vectors

The vector spatial distribution modelling was performed using both Random Forest (RF) and Boosted Regression Trees (BRT) implemented through the VECMAP® Software Suite (AVIA-GIS, Belgium), to model presence and absence, producing estimates of the probability of presence. Five replicates of each method, with a 25% holdback, were run, and the results combined to produce ensemble mean, median, minimum and maximum predictions of probability of presence. The combination of methods tends to reduce a tendency for BRT to overfit, especially for training data covering relatively restricted areas such as that available for *H. lusitanicum*.

These methods require approximately equal numbers of presence and absence points to be offered to each modelling run. The occurrence data were obtained primarily from VectorNet [22] shown in Supplementary Figure 10, supplemented by a very limited number of records from the Global Biodiversity Information Facility (GBIF, https://www.gbif.org). The VectorNet data consisted of both point and polygon data, differentiated into present, absent and introduced categories. This last category represents records of temporary presence – often from migratory birds and are not indicative of established populations. They were therefore discarded. Five points were defined for each polygon and assigned as present or absent according to the polygon status, and to these were added any point data from either VectorNet or GBIF.

The available vector data did not include the requisite number of absence points, so these needed to be generated. There are a number of geostatistical ways absences can be generated (as used for the disease modelling below), but for these vectors, it has been possible to produce habitat suitability layers based on environmental thresholds. This means that, for vectors, it is possible to assign absences to areas defined as unsuitable.

A location was defined as suitable for each vector as indicated in Supplementary Table 1, and mapped in Supplementary Figure 11. These were taken from a number of published sources [21,25–32] and from personal communications with expert colleagues. While both species do well in most woodland, grassland, shrubland and cropland environments, only *H. lusitanicum* occupies dense woodland and only *H. marginatum* is associated with sparse vegetation. Though *H. marginatum* does require minimum temperatures though the summer and needs relatively moist conditions, *H. lusitanicum* is able to occupy areas with hotter and drier summer conditions and requires a relatively warm autumn.

Once the ecologically suitable and unsuitable areas had been defined, and following the methodology used in Wint et al. (2020) [23], for *H. lusitanicum*, absence points were randomly assigned to unsuitable areas within approximately 300km of known presences, and to all areas, irrespective of suitability further away. For *H. marginatum*, absence points were randomly assigned to unsuitable areas inside the range depicted by Kolonin (2009) [20] and within approximately 300km of known presences, and to all areas, irrespective of suitability further away.

All points were then aggregated to a 10-km grid, to combine any multiple overlapping records. The number of presence and absence points was then adjusted by reducing the number of the larger class (in this case absences) to that of the less frequent class to produce a final balanced output dataset for spatial modelling. These are shown in Figure 1.

Figure 1. Points used for modelling of tick vectors

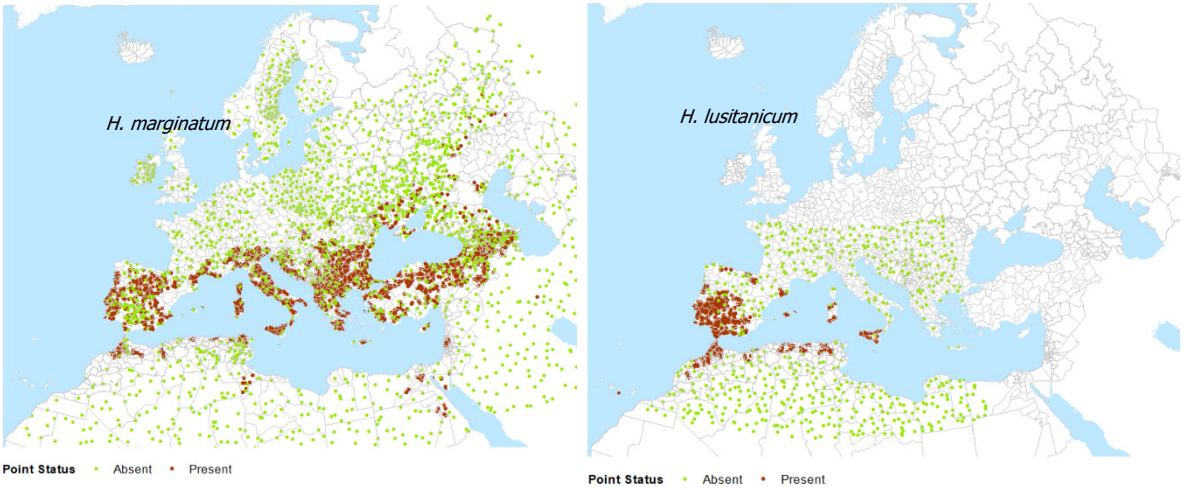

Left H. marginatum*, Right* H. lusitanicum*. Brown is presence, green is absence*

Human cases of Crimean-Congo haemorrhagic fever

An occurrence database comprising point (e.g. town or city) or polygon (e.g. county or province) locations of confirmed human CCHF infection presence was compiled from peer-reviewed literature, Genbank records, and ProMed Mail reports (https://promedmail.org). Searches were completed on 6 July 2022 and a full list of peer-reviewed citation references for all sources is provided alongside this report. A literature search was conducted on PubMed using the terms 'CCHF' or 'Crimean Congo Hemorrhagic Fever' or 'Crimean Hemorrhagic Fever' or 'Congo Hemorrhagic Fever', as well as their UK English spelling equivalents (spelled 'haemorrhagic') to capture all case reports which had been published at the time of the search. The same terms were used to search Genbank. An occurrence was defined as one or more laboratory confirmed human CCHF infection(s) occurring at a unique location (the same administrative area or 1×1km pixel for points) within one calendar year.

All occurrence data were manually reviewed, and quality controlled to ensure information fidelity and precise geo-positioning. Reports of autochthonous (locally transmitted) cases or outbreaks were entered as an occurrence within the country in which transmission occurred. If imported cases were reported with information about the site of infection, they were geo-positioned to the country where transmission occurred. Imported cases were reported with no location, they were not entered into the database. In addition, administrative area polygons greater than one square degree in area (which is approximately 12 300 km^2 at the equator) were removed from the database, as their inclusion in niche modelling would introduce a large amount of spatial imprecision.

Figure 2. Frequency histograms of CCHF human occurrence by year of published report

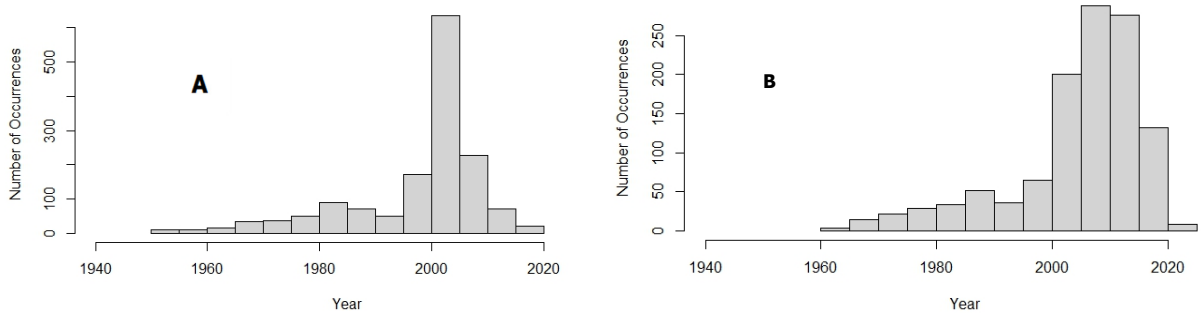

Histograms by year of (A) point occurrence locations; (B) administrative area (polygon) occurrence locations

In total, 1 437 point occurrence records and 854 polygon occurrence records were included in our final dataset after performing all quality control procedures (Supplementary Figure 12 for global map). These publications spanned the years 1953 through to July 2022. We assumed that any recorded location of presumed autochthonous human CCHF occurrence, regardless of the date of the record, represented an environment permissible for the transmission of human disease cases. Figure 2 shows histograms for the number of CCHF occurrence locations extracted from the literature by year of publication. Occurrence points identified for the original paper and for this revision together with generated pseudo-absence locations (described in greater detail below) for Europe are shown in Figure 3.

Figure 3. Occurrence and pseudo-absence locations of Crimean-Congo haemorrhagic fever human cases (Europe and neighbouring areas)

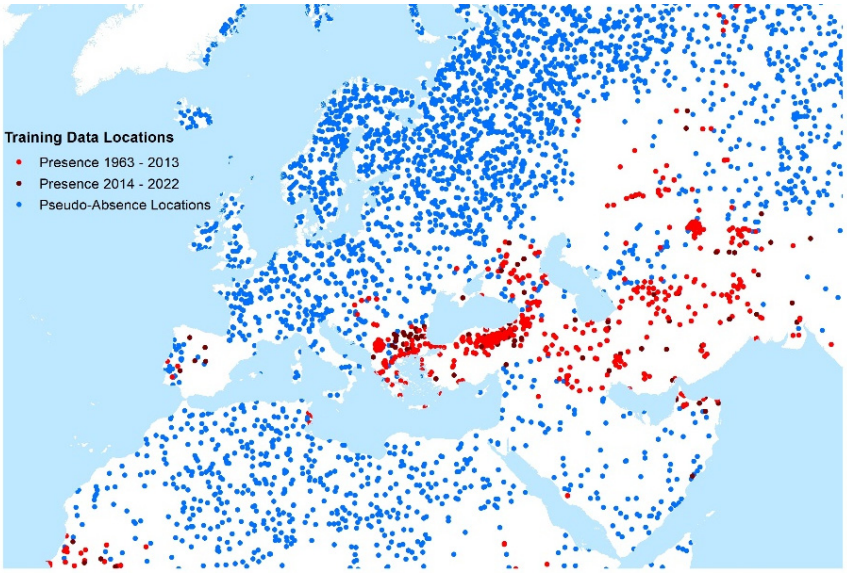

Global gridded data (1 km×1 km) were taken from the covariate data suite (Supplementary Table 2) for a set of four explanatory covariates. The covariates were chosen based on factors known or hypothesised to contribute to suitability for CCHFV transmission to humans based upon the national-level studies described in the introduction. These included: i) annual mean precipitation interpolated from global meteorological stations, and ii) mean land surface temperature derived from NASA's moderate resolution imaging spectrometer (MODIS) imagery, intended to capture the generally warm and arid climate zones where CCHFV is transmitted; iii) 1 km resolution measure of the mean annual Enhanced Vegetation Index (EVI, also from MODIS); and iv) the proportion of each 1 km×1 km grid cell covered by shrub or grass land cover types derived from the Earthenv consensus land cover datasets. No covariate grids were shown to be adversely affected by multicollinearity.

Having assembled occurrence and covariate datasets, a BRT approach was used to establish a multivariate empirical relationship between the probability of CCHF presence and the environmental conditions (as determined by the set of covariates described above) sampled at each occurrence location for points, or averaged within each polygon-level occurrence, as mentioned above for the vector modelling, BRT models require not only presence data but also pseudo-absence data defining areas of potentially unsuitable environmental conditions at unsampled locations, since data on absence of human disease are rarely reported.

Figure 4. Evidence consensus map for human Crimean-Congo haemorrhagic fever presence or absence by country

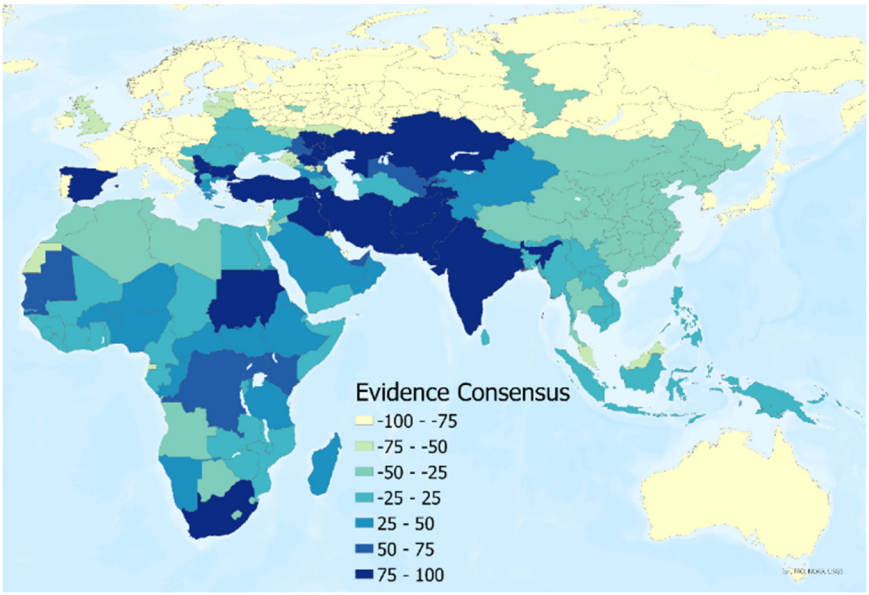

An evidence-based probabilistic framework for generating pseudo-absence data were used (Figure 4). To represent the environmental conditions in locations where human disease has not been reported, 5 000 background points were randomly generated and weighted based on a continuous raster surface derived from a national (and sometimes sub-national) CCHF evidence consensus score. This score is derived from a series of evidence types for presence aggregated and ranked from -100 (consensus on absence) to +100 (consensus on presence) as described in Messina et al [1]. More background absence points were assigned to areas with high consensus on absence.

To increase the robustness of model predictions and quantify model uncertainty, BRT models were fitted to fifty separate bootstraps of the data. We then evaluated the central tendency as the mean across all 50 BRT models. Each of the 50 individual models was fitted using the ***gbm.step*** subroutine in the ***dismo*** package in the R statistical programming environment. All other tuning parameters of the algorithm were retained as in Messina et al [1].

Results

Vector distributions

Predicted presence (and absence) for each vector species are shown in Figure 5. Three estimates of presence were derived from the model replicates – the mean, minimum and maximum values, each coded as present if the calculated probability of presence value exceeds 0.5. This resulted in four distribution categories in each map: minimum, mean and maximum predicted vector extent, and absence. All are delimited by the suitability limits described in the methods above.

The vector models generally reflect the training data well, especially for *H. lusitanicum* where sensitivity and specificity of the RF models both average well above 0.9 and the receiver operating characteristic (ROC) values of the BRT models exceed 0.95. This is perhaps to be expected as the species range is relatively restricted and less environmentally heterogeneous than that of *H. marginatum*. The *H. marginatum* models also perform well with associated Kappa values of >0.84 for the RF models and ROC values > 0.89 for the BRT models. While these models have a high sensitivity (> 0.83), their specificity is a little lower at 0.69–0.72, meaning that the models predicted a significant number of false negatives. These are largely to the East of the modelled area and outside the project area of interest – and are further discussed below.

The range of predicted vector distributions is shown by the minimum and maximum predicted extent (Figure 5): the maximum predicted extent for *H. marginatum* extends substantially further north into parts France, central Europe and the Caucasus than do the mean predictions.

Figure 5. Predicted vector distribution maps

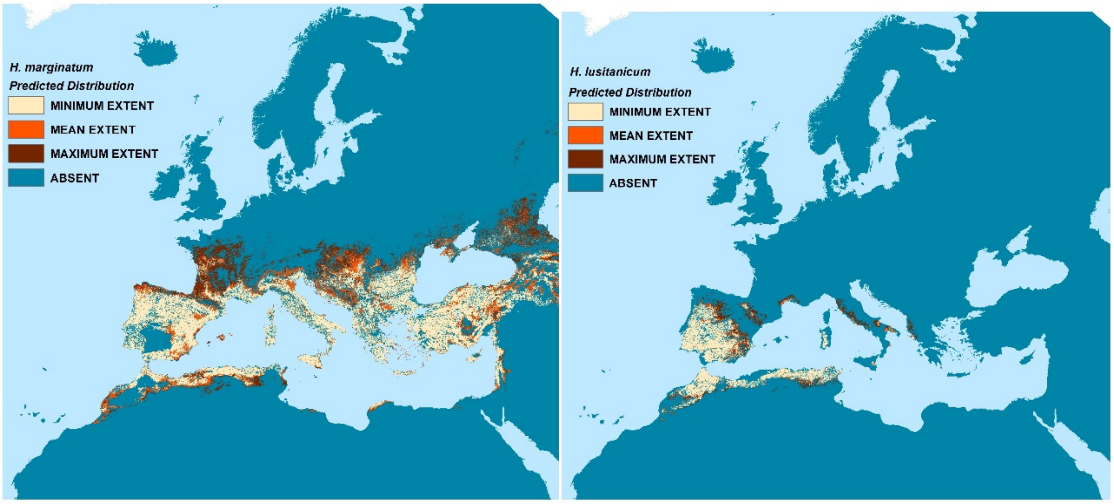

The most frequently used predictors in models for *H. marginatum* are a) the minimum values of the Normalised Difference Vegetation Index (NDVI) b) aspects of the day and night-time temperature, c) timing and levels of rainfall and d) aspects of minimum relative humidity. For *H. lusitanicum*, the best predictors relate to a) monthly rainfall seasonality and the degree to which it varies over the year; and b) the levels and timing of day and night-time temperature. The importance of the top ten predictors for each vector and modelling method is given in Supplementary Table 3.

CCHF distribution in humans

Figure 6 shows the resulting mean predictions for probability of autochthonous CCHF occurrence (ranging 0–1), displayed with minimum, maximum, and mean predicted vector presence (where at least one of the modelled probability values for either vector's presence was greater than or equal to 0.5) used as masks to hide ecologically suitable areas from view where the vectors are not predicted to be present, as well as the version without masking. Supplementary Figure 13 shows the full global modelled distribution (beyond Europe; unmasked). Uncertainty estimates for each pixel were possible from the ensemble approach (by using the interquartile range of all 50 predictions), and are shown in Supplementary Figure 14.

Figure 6. Maps of predicted ecological suitability for autochthonous human CCHF

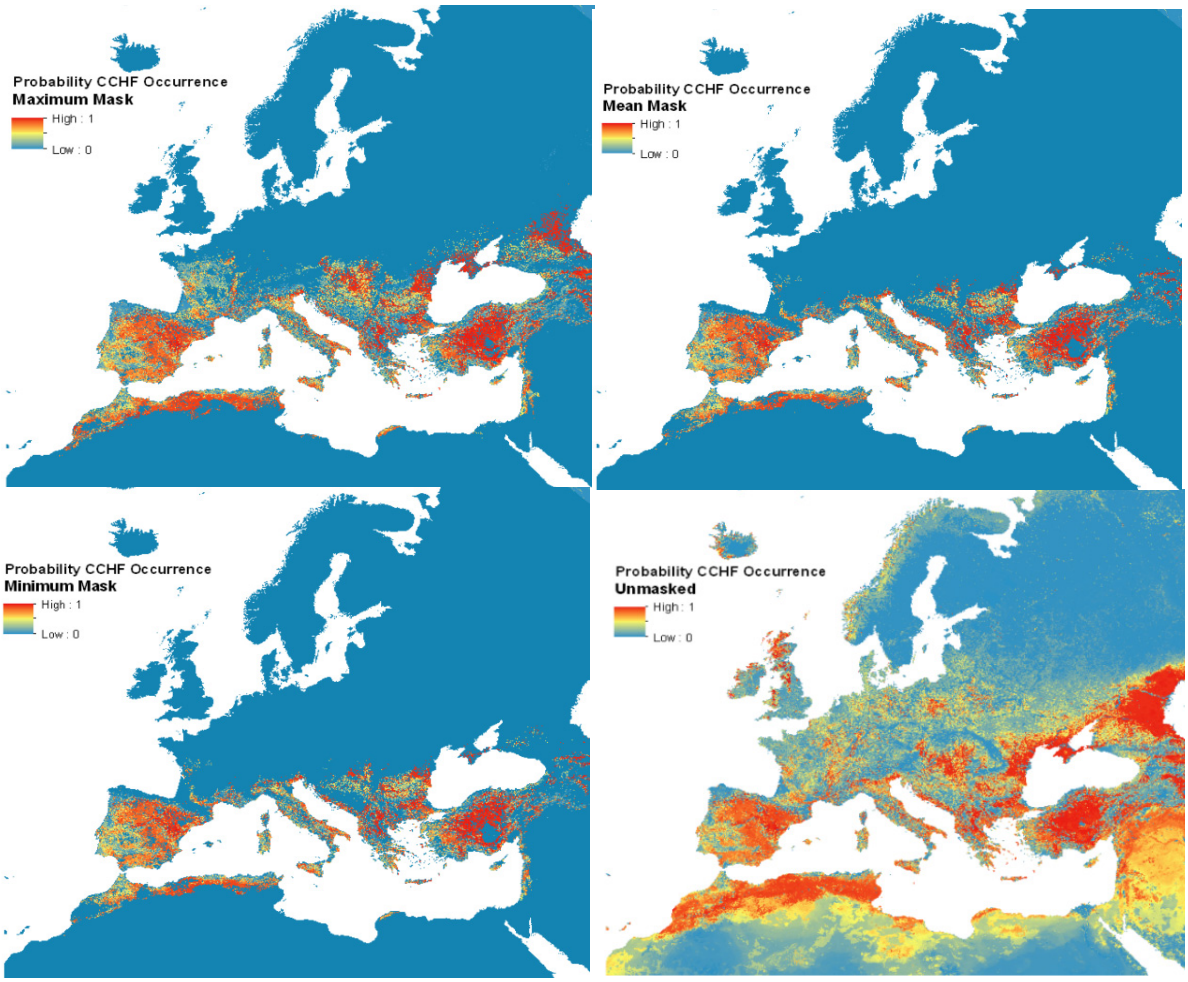

Top left: masked limiting CCHF occurrence predictions to the maximum vector extent layer; Top right: masked limiting CCHF occurrence predictions to the mean vector extent layer; Bottom left: masked limiting CCHF occurrence predictions to the minimum vector extent layer; Bottom right: CCHF occurrence predictions without mask

The disease prediction maps without masking suggest that the environmental suitability for the acquisition of autochthonous disease extends well into northern Europe and the northern Caucasus – far beyond the distributions of the two vector species considered. Limiting the predictions to the area covered by the vector distributions implies at best (mask with minimum vector distribution area) that Mediterranean France, Spain, the Balkans, Türkiye, and much of the Mediterranean seaboard are all predicted to have patches suitable for the disease.

Looking at the recorded disease locations (Supplementary Figure 12), which extend well into the Caucasus and central Europe, it seems that the CCHF ecological suitability map that used the vector mask with the maximum predicted vector distribution extents to hide areas from view where the vector is not present, provides the closest match to the known data, with suitability in e.g. Hungary and Ukraine. This level of masking suggests the predicted disease range extends significantly further north to about 49°N (in north central France and central Europe). It is also evident that the vector masking 'removes' predicted disease occurrence from Israel, Palestine, Lebanon, Syria, and Iraq. These are areas for which there are no presence records of either vector, and are also not predicted to support either vector.

Because in these maps, areas where the consensus layer (Fig. 4) suggests less than high consensus about CCHF presence are not hidden from view, the maps show France and Italy as having a high probability of CCHF, even though there have not been any reports of cases thus far. Still, Figure 6 shows several patches of environmental suitability within the predicted vector ranges in these countries. Currently, northern Europe is not predicted to be ecologically suitable for autochthonous CCHF acquisition due to a lack of vector presence.

Supplementary Figure 13 shows the probability of CCHF occurrence for the full modelled extent, without masking (i.e. no hiding of areas without vector presence or with low consensus from view). Uncertainty estimates for the updated CCHF probability of occurrence maps for each pixel were possible from the ensemble approach (by using the interquartile range of all 50 predictions) and are shown in Supplementary Figure 14.

The proportional influence of covariates towards the probability predictions in the ensemble of models is shown in Figure 7, with the total proportion equalling 100 percent. The average Area Under the Curve (AUC) across all models was 0.74 (range 0.67–0.79). AUC ranges from 0 to 1 (with an AUC of 0.5 being as good as a random prediction), and provides an aggregate measure of performance across all possible classification thresholds. Values closer to 1 indicate better model fit. Land surface temperature was by far the greatest contributor to the models, followed by precipitation, shrub land cover, and then EVI.

Figure 7. Proportional influence of covariates on CCHF suitability predictions

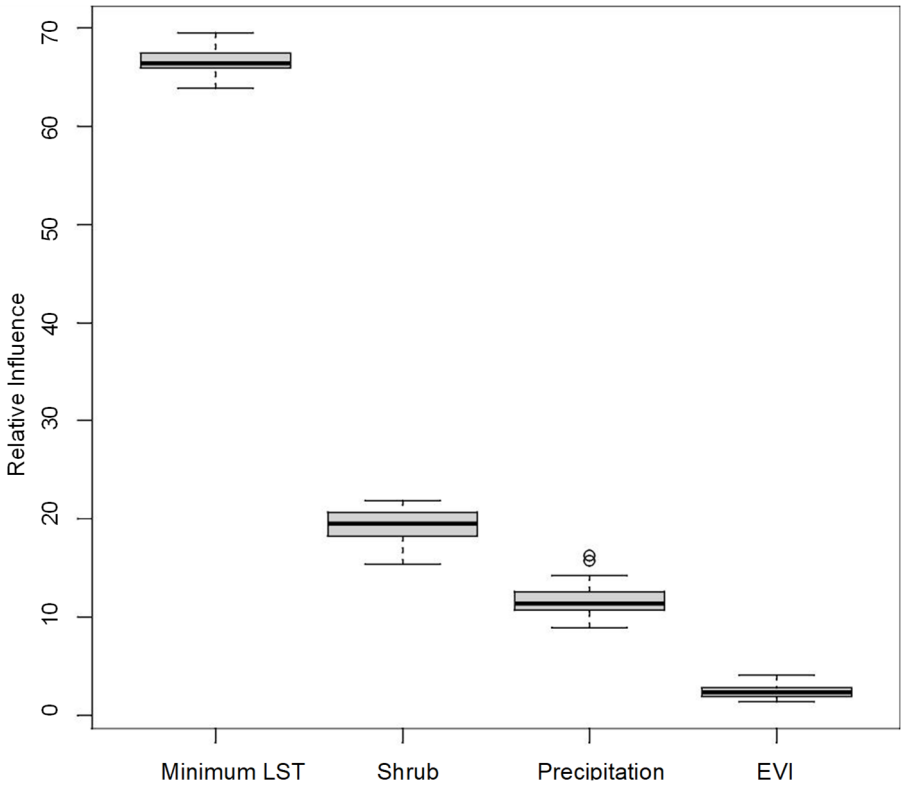

The difference between the predictions for 2022 and 2015 (Supplementary Figure 13 and 15) is presented in Figure 8, where areas without vector presence according to the maximum predicted vector extent are hidden from view – the red areas indicating where the current model predicts substantially higher ecological suitability for CCHF. This reflects the additional CCHFV presence records included in the current models in the eastern part of the region (Supplementary Figure 12). While much of Europe's predicted ecological suitability remains the same in this updated model, much of the south is predicted to be substantially more suitable: particularly pockets throughout Spain, France, Italy, the Balkans, Türkiye, and northern Africa.

Figure 8. Difference in probability of CCHF suitability predictions between 2015 and 2022 models

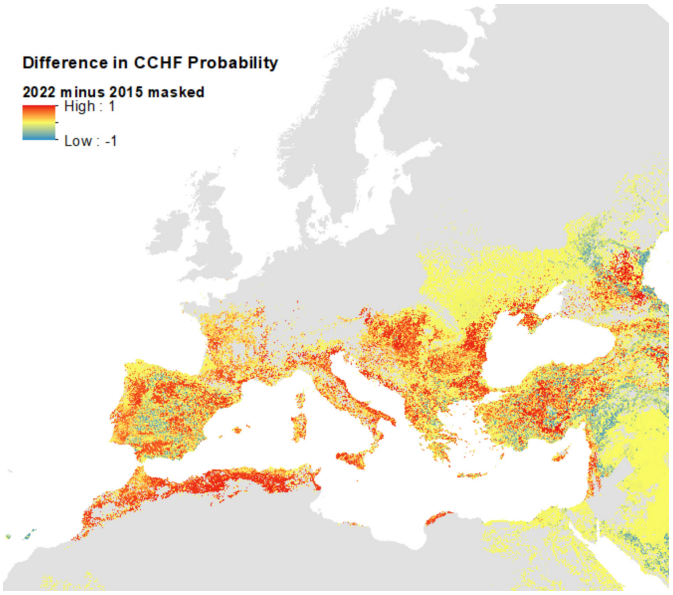

As emphasised above, this difference reflects the addition of new training data for the 2022 model. It should perhaps be noted that the two models were run at different spatial resolutions (2015 at 5km and 2022 at 1km), and so the differences are not strictly valid at the higher resolution, and the map in Figure 8 should only be used for reference on general areas where ecological suitability predictions are different.

Data availability

All spatial data inputs and outputs are provided as two ARCGIS 10.8 Packages: 1) 'VNEREGOCCHF_Vector_Report_VectorCCHFData_April23.mpk' containing the input and output Vector and CCHF datasets; and 2) VNEREGOCCHF_Vector_Report_CovariateData_April23.mpk. The CCHF data locations are also provided in and excel file 'CCHF Locations.xlsx'. The files can be downloaded here: https://drive.google.com/drive/folders/1B9LE3259ZL2NPm3kUkrVaB2e8zmM_hC4. Individual file descriptions are given in the package's Table of Contents, and the associated filenames can be obtained from the Layer Properties Source Tab. An endnote library (CCHF_2013_2022.xml) provides the references for all literature searched for CCHF occurrences, and a second file (cchf_report_2023_final.xml) provides all references cited in the report.

Discussion

This report provides updated baseline data for monitoring future changes in the distribution of autochthonous CCHF and its associated vectors for Europe and its neighbouring areas. The predicted distributions suggest that a number of countries that have yet to record CCHF have areas that are environmentally suitable for autochthonous disease – most especially those with Mediterranean coastlines (France, Italy, the southern Balkans, western Asia and northern Africa). Both the ecological CCHF suitability predictions and the maximum predicted extents of the two vector species imply a potential CCHF distribution extending significantly further northward into mainland western and central Europe. It is tempting to suggest that this northward shift could be driven by a warming climate. It is also worth noting that these maximum predicted extents overlap some of the VectorNet distributions assigned as 'introduced' (Supplementary Figure 10) because they are thought to be too far beyond the current northern distribution limits to represent established populations. It could be that these introduced presence points are in fact the first harbingers of future spread and establishment.

Further cartographic refinements are required in order to help differentiate endemic from epidemic-prone areas, particularly in areas where there is less certainty about the presence or absence of CCHFV overall. The CCHF occurrence database used in creating the CCHF ecological suitability map has been updated for to mid-2022, and can continue to be updated with new information as it becomes available. Other potential improvements are the inclusion of other potential CCHFV vector species into the masking process (discussed below) and the addition of more data types, such as those related to CCHFV seroprevalence. For the latter, recent research has elucidated potentially important CCHFV reservoir species in non-endemic areas (e.g. France, Italy) that should also be considered; for example, imported sheep and goats that may be more susceptible to CCHFV infection [33,34]. These efforts to improve mapping of current ecological suitability could further facilitate identification of potential transmission foci.

Figure 9. Maps of high predicted Crimean-Congo haemorrhagic fever suitability

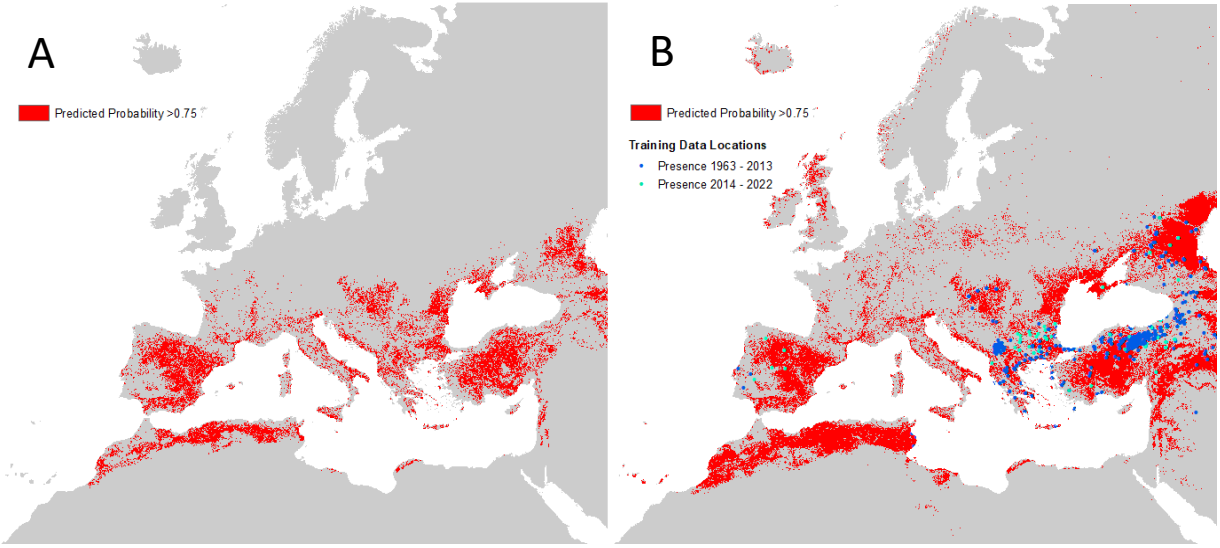

A) Left: areas with predicted probability of disease >= 0.75 limited to the maximum predicted vector extent; B) Right: same as left but with recorded occurrence points and not restricted to areas where the vectors are present.

Already, these maps have been improved from the 2015 Messina et al. [1] versions due to not only the updated occurrence database and higher spatial resolution (now 1km x 1km), which includes significant new data from Türkiye, Spain and the Caucasus, but also the inclusion of vector suitability instead of Evidence Consensus to mask disease predictions. Panel A of Figure 9 shows areas where the CCHF probability of occurrence is high (greater than or equal to 0.75) within the maximum predicted presence area of either suitable vector species. As such, these figures may be used as a guide for prioritising future virus surveillance efforts in humans and animals. Although a similar occurrence dataset was used in the current model and that of Okely et al. (2020) [2], our predictions do not have the high ecological suitability in Poland demonstrated in their maps; in contrast, greater ecological suitability for CCHFV is seen in southern Russia and Kazakhstan. This is likely to be due to the different set of covariates used in each set of models (for example, Okely et al. used a Principal Components Analysis to reduce all available bioclimatic variables to a small number of factors, while our models selected those considered most important according to the literature, as well as a measure of shrub land cover). The equivalent high probability maps for each vector species are presented in Supplementary Figure 16. It can be seen that areas bordering the Adriatic and Mediterranean Seas are likely to be particularly important for vector and disease surveillance, as well as the majority of the Iberian peninsula and Türkiye.

It is worth noting that the map of CCHF suitability unrestricted by the presence area of vector species (Figure 9, Panel B) suggests many areas (e.g. Scotland) to be environmentally suitable for CCHF occurrence that are far beyond recorded occurrence locations and the predicted range of the two vector species. This underlines the need for delimiting the predictions to within the area where the vectors are present to produce a realistic disease prediction but does also suggest that if the vectors spread to these areas, then the disease might as well.

While the predicted vector and vector-masked disease outputs reflect the known data well for most of the area of interest, recorded (and unmasked predicted) disease occurrence in certain parts of Western Asia is probably incorrectly hidden from view by the vector distribution mask. The literature reports *H. marginatum* to be present (widespread) in Iran [20,35,36], further south than the distribution range boundary predicted by Kolonin [20], so it is likely that the point data available is substantially underrepresented for these regions (Iraq and Iran are not inside the region covered by VectorNet) and also perhaps some of the CCHF pseudoabsences were incorrectly placed in suitable areas in this region. Otherwise, it may be that the vector (and thus the virus in vectors) is present in pockets (perhaps of irrigation) that these spatial suitability models do not 'detect'. If so, this suggests that the unmasked disease models are more reliable in such areas. Also, a number of other *Hyalomma* species including *H. impeltatum*, *H. anatolicum*, *H. asiaticum* , *H. excavatum* and *H. dromedarii* have been identified as CCHFV vectors in Iran and its neighbours [20,37]. These are not present in Europe (and there are few if any geo-referenced occurrence records) and were not incorporated into the vector masking – with the main focus being on Europe – but could improve the prediction in Western Asia.

A further potential improvement would be delimiting the maps according to the presence area of host species for ticks, such as deer (for *H. marginatum*) and hares (for *H. lusitanicum*) and limiting surveillance priority to within rural areas and/or those which are nearer to livestock populations.

Conclusion

The updated and improved maps presented in this report could serve as a starting point for a wider discussion about the potential likelihood of occurrence of CCHF in Europe. Increasing awareness of public health experts and the medical profession in geographic areas which we have newly shown to have a high probability of disease occurrence may lead to CCHF being considered in the differential diagnosis of people with compatible symptoms (such as high fever, muscle pain, dizziness, abnormal sensitivity to light, abdominal pain, and vomiting) and a recent history of tick bite.

Future serological studies focussed in areas identified as high-risk in this report could also lead to additional occurrence records that would in turn improve models that incorporate serological data. As evidenced by reports of the disease occurring in Spain in 2016 (before which a 2015 publication did not identify this as a suitable CCHFV transmission area), it is important for the mapping of high-suitability areas to be updated regularly, taking into consideration advancements in understanding of the disease distribution, as well as new covariate data sources.

References

1. Messina JP, Pigott DM, Golding N, Duda KA, Brownstein JS, Weiss DJ, et al. The global distribution of Crimean-Congo hemorrhagic fever. Trans R Soc Trop Med Hyg. 2015;109:503–13.
2. Okely M, Anan R, Gad-Allah S, Samy AM. Mapping the environmental suitability of etiological agent and tick vectors of Crimean-Congo hemorrhagic fever. Acta Trop. 2020;203:105319.
3. Hoogstraal H. The epidemiology of tick-borne Crimean-Congo hemorrhagic fever in Asia, Europe, and Africa. J Med Entomol. 1979;15:307–417.
4. Whitehouse CA. Crimean-Congo hemorrhagic fever. Antivir Res. 2004;64:145–60.
5. Han N, Rayner S. Epidemiology and mutational analysis of global strains of Crimean-Congo haemorrhagic fever virus. Virol Sin. 2011;26:229–44.
6. Ergonul O. Crimean-Congo haemorrhagic fever. Lancet Infect Dis. 2006;6:203–14.
7. Papa A, Bino S, Llagami A, Brahimaj B, Papadimitriou E, Pavlidou V, et al. Crimean-Congo hemorrhagic fever in Albania, 2001. Eur J Clin Microbiol Infect Dis. 2002;21:603–6.
8. Karti SS, Odabasi Z, Korten V, Yilmaz M, Sonmez M, Caylan R, et al. Crimean-Congo hemorrhagic fever in Turkey. Emerg Infect Dis. 2004;10:1379–84.
9. Zakhashvili K, Tsertsvadze N, Chikviladze T, Jghenti E, Bekaia M, Kuchuloria T, et al. Crimean-Congo hemorrhagic fever in man, Republic of Georgia, 2009. Emerg Infect Dis. 2010;16:1326–8.
10. European Centre for Disease Prevention and Control (ECDC). Cases of Crimean-Congo haemorrhagic fever in the EU/EEA, 2013–present. Available at: https://www.ecdc.europa.eu/en/crimean-congo-haemorrhagic-fever/surveillance/cases-eu-since-2013
11. Maltezou HC, Andonova L, Andraghetti R, Bouloy M, Ergonul O, Jongejan F, et al. Crimean-Congo hemorrhagic fever in Europe: current situation calls for preparedness. Euro Surveill. 2010;15:19504. Available at: https://www.eurosurveillance.org/content/10.2807/ese.15.10.19504-en
12. Grard G, Drexler JF, Fair J, Muyembe JJ, Wolfe ND, Drosten C, et al. Re-emergence of Crimean-Congo hemorrhagic fever virus in Central Africa. PLoS Negl Trop Dis. 2011;5:e1350.
13. Appannanavar SB, Mishra B. An Update on Crimean Congo Hemorrhagic Fever. J Glob Infect Dis. 2011;3:285–92.
14. Maltezou HC, Papa A. Crimean-Congo hemorrhagic fever: risk for emergence of new endemic foci in Europe? Travel Med Infect Dis. 2010;8:139–43.
15. Lutomiah J, Musila L, Makio A, Ochieng C, Koka H, Chepkorir E, et al. Ticks and tick-borne viruses from livestock hosts in arid and semiarid regions of the eastern and northeastern parts of Kenya. J Med Entomol. 2014;51:269–77.
16. Okello-Onen J, Tukahirwa EM, Perry BD, Rowlands GJ, Nagda SM, Musisi G, et al. Population dynamics of ticks on indigenous cattle in a pastoral dry to semi-arid rangeland zone of Uganda. Exp Appl Acarol. 1999;23:79–88.
17. Aktas M, Altay K, Dumanli N. A molecular survey of bovine Theileria parasites among apparently healthy cattle and with a note on the distribution of ticks in eastern Turkey. Vet Parasitol. 2006;138:179–85.
18. Horak IG, Braack LE, Fourie LJ, Walker JB. Parasites of domestic and wild animals in South Africa. XXXVIII. Ixodid ticks collected from 23 wild carnivore species. Onderstepoort J Vet Res. 2000;67:239–50.
19. Negredo A, de la Calle-Prieto F, Palencia-Herrejón E, Mora-Rillo M, Astray-Mochales J, Sánchez-Seco MP, et al. Autochthonous Crimean-Congo Hemorrhagic Fever in Spain. N Engl J Med. 2017;377:154–61.
20. Kolonin G. Fauna of ixodid ticks of the world (Acari, Ixodidae). Moscow. 2009. Available at http://www.kolonin.org
21. Estrada-Peña A, Venzal J. Climate Niches of Tick Species in the Mediterranean Region: Modeling of Occurrence Data, Distributional Constraints, and Impact of Climate Change. J Med Entomol. 2007;44:1130–8.
22. Wint GRW, Balenghien T, Berriatua E, Braks M, Marsboom C, Medlock J, et al. VectorNet: collaborative mapping of arthropod disease vectors in Europe and surrounding areas since 2010. Euro Surveill. 2023;28(26):2200666. Available at: https://www.eurosurveillance.org/content/10.2807/1560-7917.ES.2023.28.26.2200666
23. Wint W, Van Bortel W, Schaffner F. RVF vector spatial distribution models: Probability of presence. EFSA Support Publ. 2020;17:1800E.
24. Scharlemann JPW, Benz D, Hay SI, Purse BV, Tatem AJ, Wint GRW, et al. Global Data for Ecology and Epidemiology: A Novel Algorithm for Temporal Fourier Processing MODIS Data. PLOS ONE. 2008;3:e1408.

25. Fernández-Ruiz N, Estrada-Peña A. Towards New Horizons: Climate Trends in Europe Increase the Environmental Suitability for Permanent Populations of Hyalomma marginatum (Ixodidae). Pathogens. 2021;10:95.
26. Kimball A, Hatfield KM, Arons M, James A, Taylor J, Spicer K, et al. Asymptomatic and Presymptomatic SARS-CoV-2 Infections in Residents of a Long-Term Care Skilled Nursing Facility - King County, Washington, March 2020. MMWR Morb Mortal Wkly Rep. 2020;69:377–81.
27. Santos-Silva MM. Hyalomma lusitanicum Koch, 1844 (Figs. 155–157). In: Estrada-Peña A, Mihalca AD, Petney TN, editors. Ticks Eur North Afr Guide Species Identif. Cham: Springer International Publishing; 2017. p. 383–7. Available at: https://doi.org/10.1007/978-3-319-63760-0_72
28. Williams HW, Cross DE, Crump HL, Drost CJ, Thomas CJ. Climate suitability for European ticks: assessing species distribution models against null models and projection under AR5 climate. Parasit Vectors. 2015;8:440.
29. Estrada-Pena A, Ayllon N, De La Fuente J. Impact of Climate Trends on Tick-Borne Pathogen Transmission. Front Physiol. 2012;3:64. Available at: https://www.frontiersin.org/articles/10.3389/fphys.2012.00064
30. Estrada-Peña A, Sánchez N, Estrada-Sánchez A. An Assessment of the Distribution and Spread of the Tick Hyalomma marginatum in the Western Palearctic Under Different Climate Scenarios. Vector-Borne Zoonotic Dis. 2012;12:758–68.
31. Estrada-Peña A, Jameson L, Medlock J, Vatansever Z, Tishkova F. Unraveling the Ecological Complexities of Tick-Associated Crimean-Congo Hemorrhagic Fever Virus Transmission: A Gap Analysis for the Western Palearctic. Vector-Borne Zoonotic Dis. 2012;12:743–52.
32. Gray JS, Dautel H, Estrada-Peña A, Kahl O, Lindgren E. Effects of climate change on ticks and tick-borne diseases in Europe. Interdiscip Perspect Infect Dis. 2009;2009:593232.
33. Spengler JR, Bergeron É, Rollin PE. Seroepidemiological Studies of Crimean-Congo Hemorrhagic Fever Virus in Domestic and Wild Animals. PLoS Negl Trop Dis. 2016;10:e0004210.
34. Grech-Angelini S, Lancelot R, Ferraris O, Peyrefitte CN, Vachiery N, Pédarrieu A, et al. Crimean-Congo Hemorrhagic Fever Virus Antibodies among Livestock on Corsica, France, 2014–2016. Emerg Infect Dis. 2020;26:1041–4.
35. Kadir MA, Zangana IK, Mustafa BHS. A study on epidemiology of hard tick (Ixodidae) in sheep in Sulaimani governorate - Iraq. Iraqi J Vet Sci. 2012;26:95–103.
36. Ismael S, Omer LT. Molecular identification of new circulating Hyalomma asiaticum asiaticum from sheep and goats in Duhok governorate, Iraq. Iraqi J Vet Sci. 2021;35:79–83.
37. Telmadarraiy Z, Chinikar S, Vatandoost H, Faghihi F, Hosseini-Chegeni A. Vectors of Crimean Congo Hemorrhagic Fever Virus in Iran. J Arthropod-Borne Dis. 2015;9:137–47.
38. Kraemer MUG, Reiner RC, Brady OJ, Messina JP, Gilbert M, Pigott DM, et al. Past and future spread of the arbovirus vectors Aedes aegypti and Aedes albopictus. Nat Microbiol. 2019;4:854–63.

Annex

Supplementary Table 1. Vector habitat suitability conditions

Variable	*H. marginatum*	*H. lusitanicum*	Dataset
Forest/woodland > 40%	No	Yes	Corine/ESA CCI
Woodland or Forest 15 - 40%	Yes	Yes	Corine/ESA CCI
Shrubland/Grassland	Yes	Yes	Corine/ESA CCI
Cropland	Yes	Yes	Corine/ESA CCI
Sparse Vegetation	Yes	No	Corine/ESA CCI
Minimum Elevation	< 2000m	< 2000m	GMTED (see URL below)
Max temp	< 35 °C	< 40 °C	Worldclim (see URL below)
Summer minimum Relative Humidity		>10%, < 65%	Derived from MODIS LST (see URL below)
Cumulative temperature above 15°C, April to August	>800, plus 50km buffer		Worldclim (see URL below)
Cumulative minimum temperature above 0 °C, October and November		>400	Worldclim (see URL below)
Mean Annual Vapour Pressure Deficit	< 15%		ECWMF (see URL below)

Corine Land Cover 2018: https://land.copernicus.eu/pan-european/corine-land-cover
ESA CCI Land Cover: http://maps.elie.ucl.ac.be/CCI/viewer/download.php
GMTED: https://topotools.cr.usgs.gov/gmted_viewer/gmted2010_global_grids.php
Modis Land Surface Temperature: https://modis.gsfc.nasa.gov/data/dataprod/mod11.php
Worldclim: https://www.worldclim.org/data/index.html
ECMWF: https://www.ecmwf.int/en/forecasts/datasets/reanalysis-datasets/era5

Supplementary Table 2. Covariates offered to modelling procedures

1 VCC1103A0: Middle infra-red mean	45 VCC1115MN: EVI minimum
2 VCC1103A1: Middle infra-red amplitude 1	46 VCC1115MX: EVI maximum
3 VCC1103A2: Middle infra-red amplitude 2	47 VCC1115P1: EVI phase 1
4 VCC1103A3: Middle infra-red amplitude 3	48 VCC1115P2: EVI phase 2
5 VCC1103MN: Middle infra-red minimum	49 VCC1115P3: EVI phase 3
6 VCC1103MX: Middle infra-red maximum	50 VCC1115VR: EVI variance
7 VCC1103P1: Middle infra-red phase 1	51 VCMI30GRDP1K DEM (Elevation) +1000
8 VCC1103P2: Middle infra-red phase 2	52 VC1920A0: ERA5 Precipitation mean
9 VCC1103P3: Middle infra-red phase 3	53 VC1920A1: ERA5 Precipitation amplitude 1
10 VCC1103VR: Middle infra-red variance	54 VC1920A2: ERA5 Precipitation amplitude 2
11 VCC1107A0: Daytime LST mean	55 VC1920A3: ERA5 Precipitation amplitude 3
12 VCC1107A1: Daytime LST amplitude 1	56 VC1920MN: ERA5 Precipitation minimum
13 VCC1107A2: Daytime LST amplitude 2	57 VC1920MX: ERA5 Precipitation maximum
14 VCC1107A3: Daytime LST amplitude 3	58 VC1920P1: ERA5 Precipitation phase 1
15 VCC1107MN: Daytime LST minimum	59 VC1920P2: ERA5 Precipitation phase 2
16 VCC1107MX: Daytime LST maximum	60 VC1920P3: ERA5 Precipitation phase 3
17 VCC1107P1: Daytime LST phase 1	61 VC1920VR: ERA5 Precipitation variance
18 VCC1107P2: Daytime LST phase 2	62 VCWPOPPPP: Worldpop Human Population density 2020
19 VCC1107P3: Daytime LST phase 3	63 VCV59EL500: GNTED Elevation + 500
20 VCC1107VR: Daytime LST variance	64 VCEELCBARE: consensus % bare ground
21 VCC1108A0: Nighttime LST mean	65 VCEELCDCBD3: consensus % deciduous broadleaved forest
22 VCC1108A1: Nighttime LST amplitude 1	66 VCEELCEVGBD2: consensus % evergreen broadleaved forest
23 VCC1108A2: Nighttime LST amplitude 2	67 VCEELCEVGND1: consensus % evergreen needleleaved forest
24 VCC1108A3: Nighttime LST amplitude 3	68 VCEELCFLOOD8: consensus % flooded
25 VCC1108MN: Nighttime LST minimum	69 VCEELCHVCB: consensus % herbaceous cover
26 VCC1108MX: Nighttime LST maximum	70 VCEELCMANAG7: consensus % managed land
27 VCC1108P1: Nighttime LST phase 1	71 VCEELCOTHTR4: consensus % other land cover
28 VCC1108P2: Nighttime LST phase 2	72 VCEELCSHRUB5: consensus % shrub cover
29 VCC1108P3: Nighttime LST phase 3	73 VCEELCURB9: consensus % urban
30 VCC1108VR: Nighttime LST variance	74 VCEELCWATER12: consensus % water
31 VCC1114A0: NDVI mean	75 VC82094A0: Relative Humidity mean
32 VCC1114A1: NDVI amplitude 1	76 VC82094A1: Relative Humidity amplitude 1
33 VCC1114A2: NDVI amplitude 2	77 VC82094A2: Relative Humidity amplitude 2
34 VCC1114A3: NDVI amplitude 3	78 VC82094A3: Relative Humidity amplitude 3
35 VCC1114MN: NDVI minimum	79 VC82094MN: Relative Humidity minimum
36 VCC1114MX: NDVI maximum	80 VC82094MX: Relative Humidity maximum
37 VCC1114P1: NDVI phase 1	81 VC82094P1: Relative Humidity phase 1
38 VCC1114P2: NDVI phase 2	82 VC82094P2: Relative Humidity phase 2
39 VCC1114P3: NDVI phase 3	83 VC82094P3: Relative Humidity phase 3
40 VCC1114VR: NDVI variance	84VC82094VR: Relative Humidity variance
41 VCC1115A0: EVI mean	
42 VCC1115A1: EVI amplitude 1	
43 VCC1115A2: EVI amplitude 2	
44 VCC1115A3: EVI amplitude 3	

LST: Land Surface Temperature; NDVI: Normalised Difference vegetation Index; EVI: Enhanced Vegetation Index; DEM: Digital Elevation Model. All files starting with VCC11, VC19 and VC82 are Fourier processed MODIS Satellite Imagery produced by the Environmental Research Group Oxford according to the methods set out in Scharlemann et. al. (2008) [24].
The Relative Humidity layers were produced as described in n Kraemer et. al. (2019) [38] and then Fourier Processed as described above.
The Elevation layer was extracted from the GMTED datasets (https://topotools.cr.usgs.gov/gmted_viewer/gmted2010_global_grids.php) and the negative values removed by adding 1 000.
Population layers derived from layers produced by worldpop (https://www.worldpop.org/datacatalog)
All Files with VCEELC in file name were derived from the Earthenv consensus land cover data product (https://www.earthenv.org/landcover)
All layers extracted and standardised by ERGO for MOOD Horizon 2020 project N° 874850 (https://mood-h202.eu)

Supplementary Figure 10. VectorNet data locations

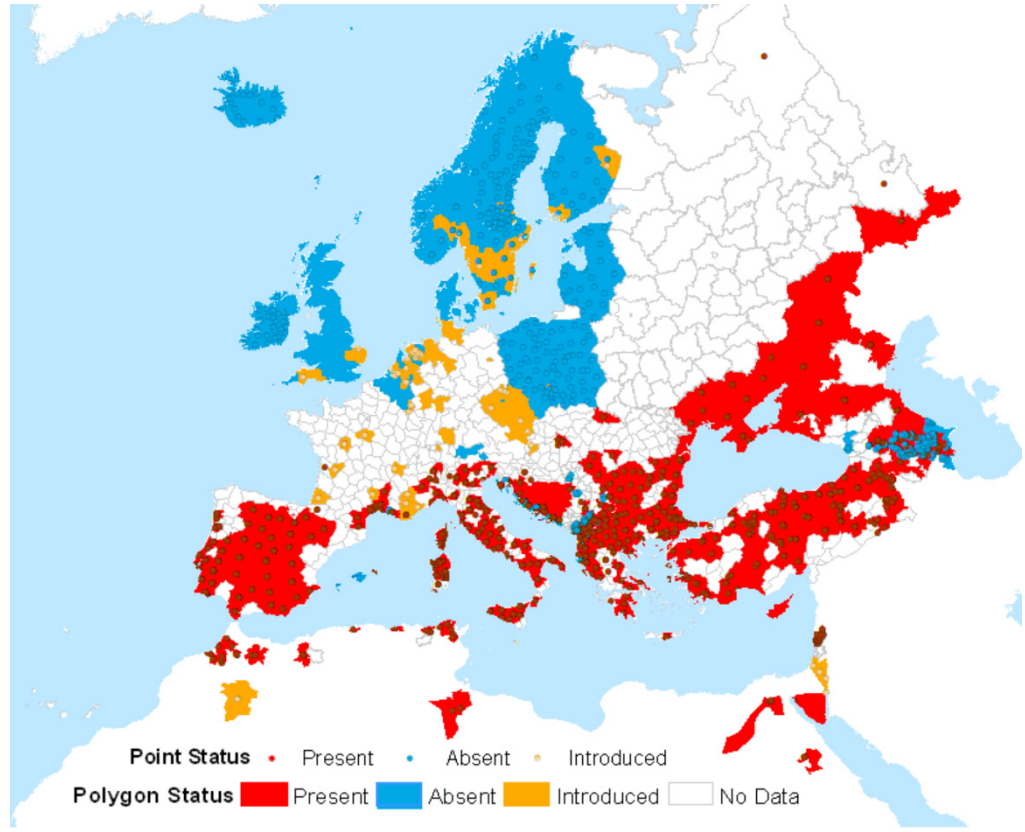

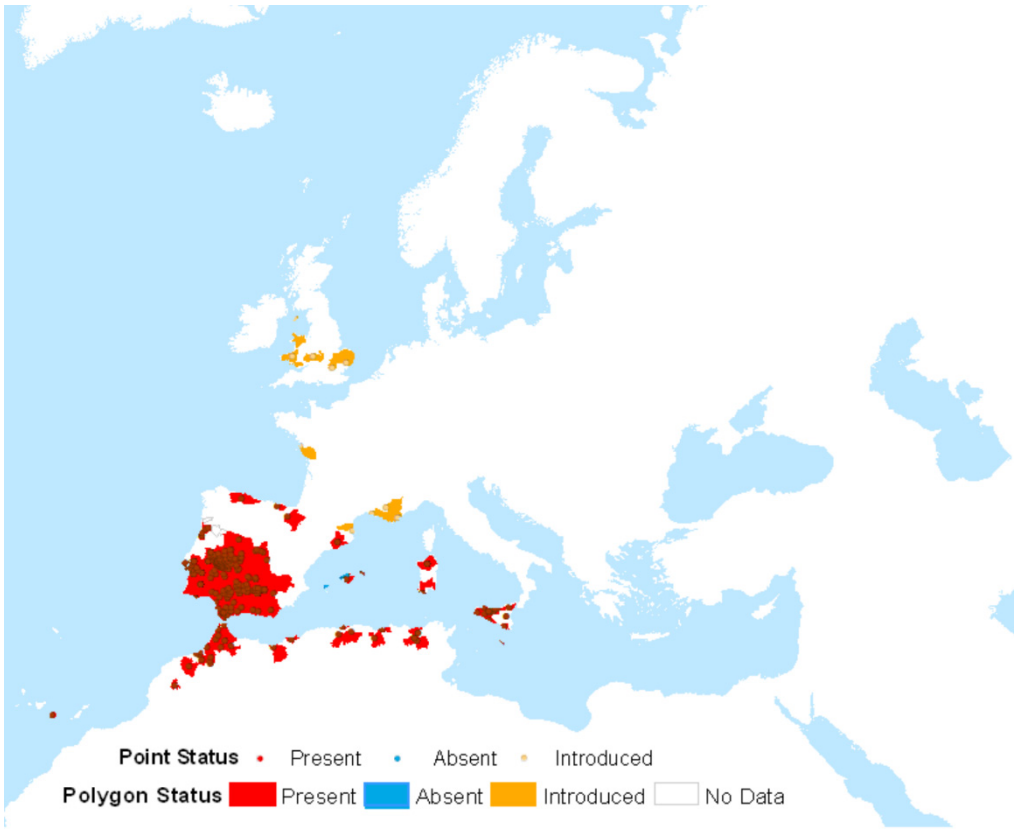

Top: H. marginatum*; bottom:* H. lusitanicum

Supplementary Figure 11. Habitat suitability for each vector

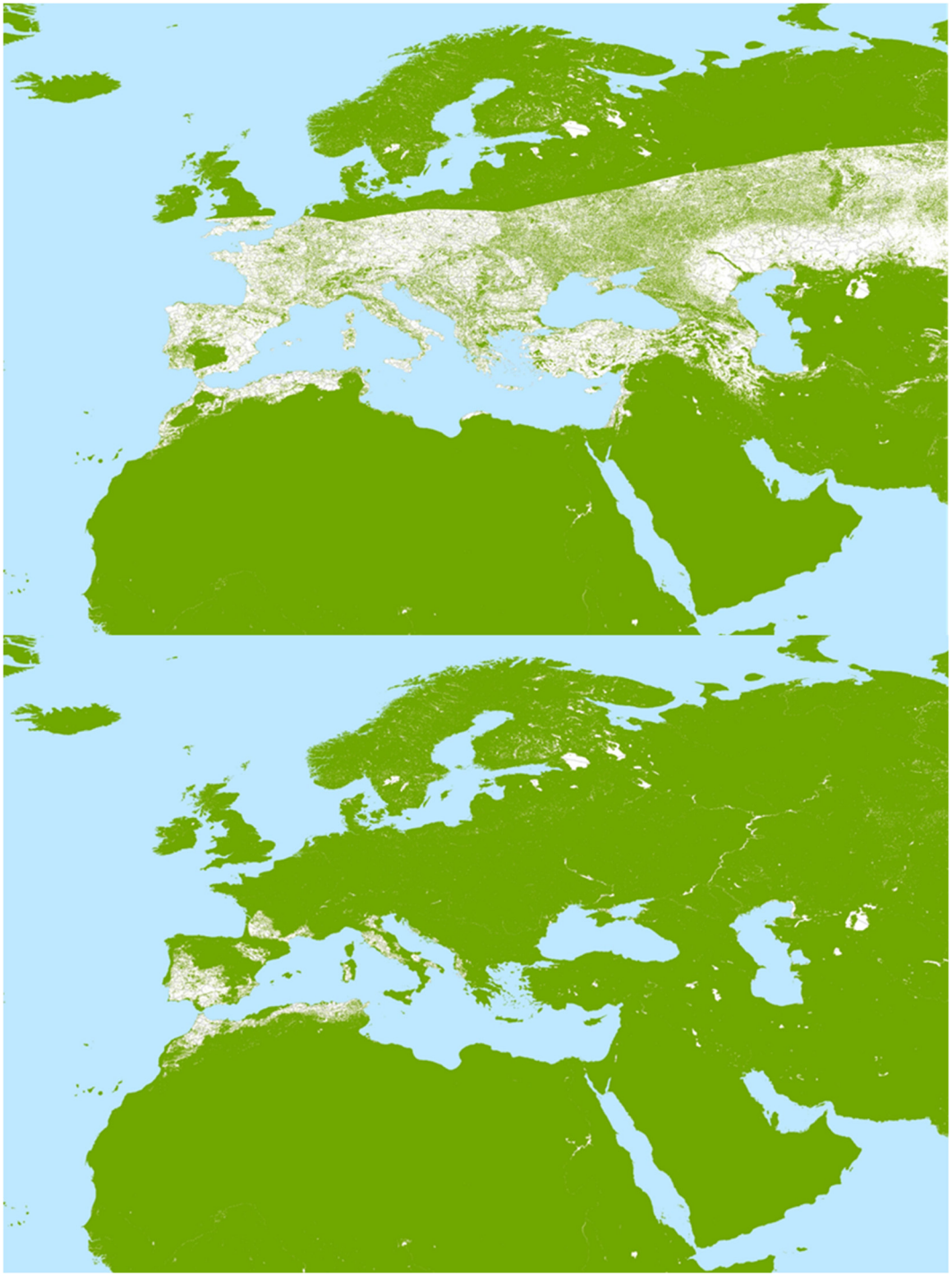

Top: H. marginatum*; bottom:* H. lusitanicum. *Green: unsuitable; white: suitable.*

Supplementary Figure 12. Full extent of Crimean-Congo haemorrhagic fever pseudo-absence and occurrence locations

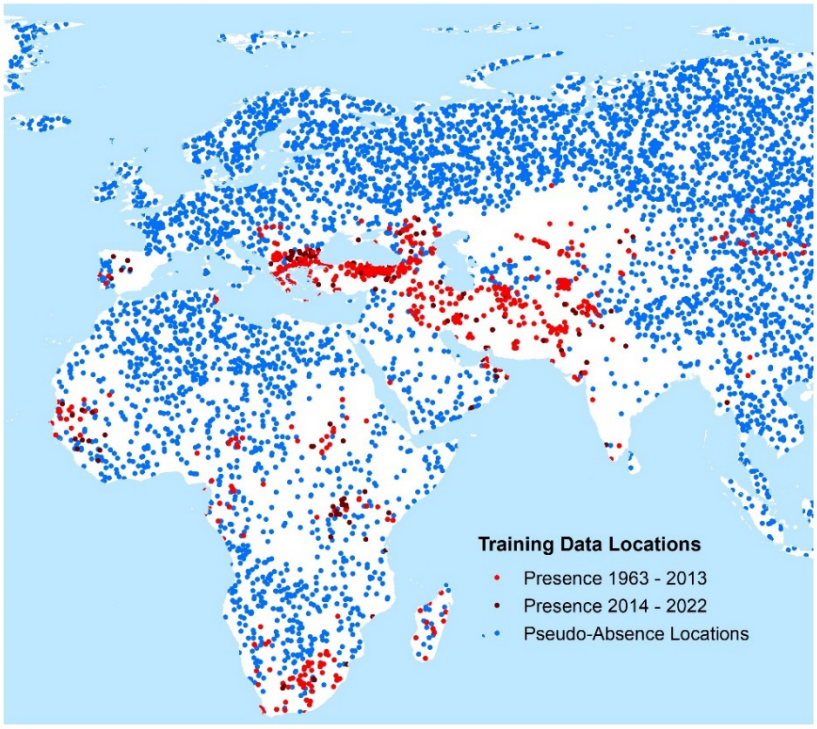

Supplementary Table 3. Top 10 vector model predictors

	H. lusitanicum				*H. marginatum*		
RF		BRT		RF		BRT	
Predictor	Metric*	Predictor	Metric	Predictor	Metric	Predictor	Metric
Rainfall Amplitude Component 1	20.44	Rainfall Amplitude Component 1	2.57	NDVI Minimum	9.84	Day Temperature Mean	1.66
Day Temperature Phase Component 2	17.2	Rainfall Amplitude Component 2	2.45	Rainfall Amplitude Component 2	9.8	NDVI Minimum	1.62
Rainfall Minimum	11.68	Day Temperature Phase Component 2	2.17	Day Temperature Mean	7.3	Rainfall Amplitude Component 2	1.55
Night Temperature Amplitude Component 1	7.1	Infra Red Amplitude Component 1	1.92	Rainfall Phase Component 3	4.36	Rainfall Amplitude Component 1	1.46
Night Temperature Minimum	4.12	EVI Phase Component 1	1.62	Rainfall Phase Component 1	4.34	Night Temperature Phase Component 2	1.41
Rainfall Amplitude Component 2	3.8	Infra Red Phase Component 1	1.52	Bare Ground Proportion	3.48	Night Temperature Maximum	1.35
Rainfall Phase Component 2	2.91	Night Temperature Amplitude Component 1	1.52	Night Temperature Phase Component 2	2.95	Rainfall Maximum	1.29
Infra Red Phase Component 1	2.59	Day Temperature Mean	1.4	Relative Humidity minimum	2.85	Day Temperature Phase Component 1	1.29
Night Temperature Mean	2.12	NDVI Phase Component 1	1.3	Relative Humidity Phase Component 3	2.8	NDVI Amplitude Component 2	1.26
Relative Humidity Amplitude Component 2	1.91	Infra Red Phase Component 2	1.28	Rainfall Phase Component 2	2.77	Day Temperature Maximum	1.25

**For both RF and BRT the higher the value of the metric within each method the more important the predictor. The metrics are different for each method, and should not be compared.*

Supplementary Figure 13. Full extent of modelled Crimean-Congo haemorrhagic fever suitability map

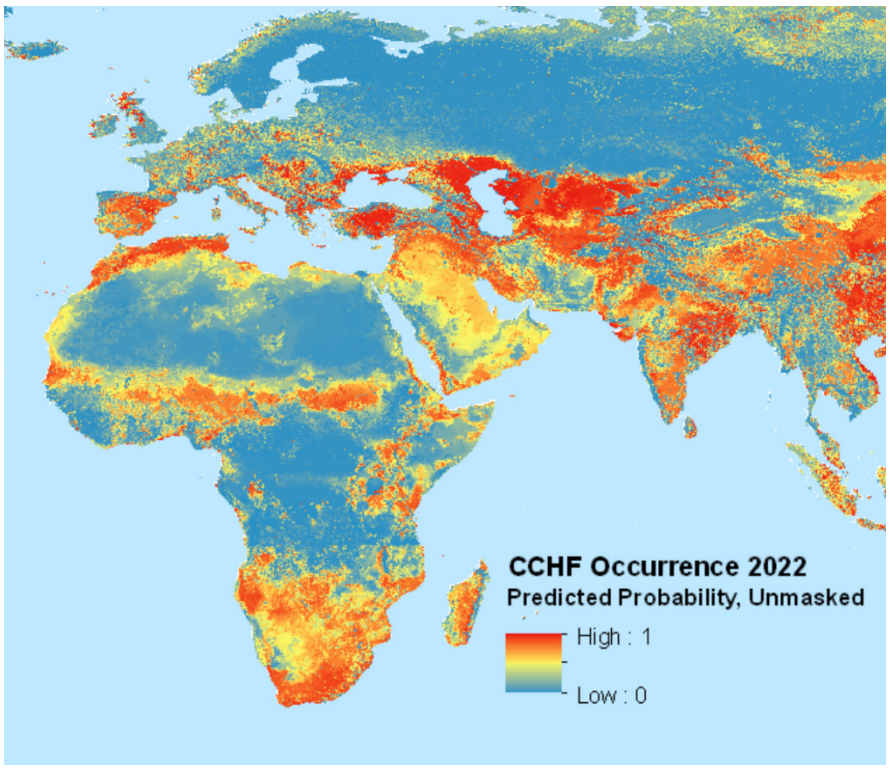

Supplementary Figure 14. Uncertainty estimates for Crimean-Congo haemorrhagic fever suitability estimates (probability of occurrence)

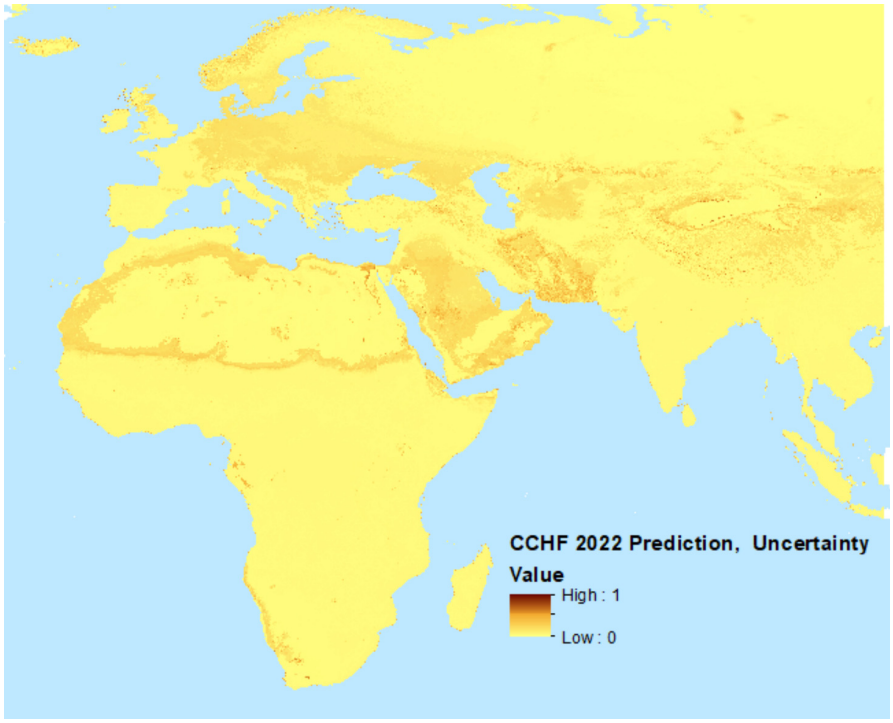

Uncertainty ranges from 0 to 1, with higher values indicating greater ranges in the estimated probability of occurrence.

Supplementary Figure 15. Unmasked 2015 Crimean-Congo haemorrhagic fever prediction from Messina et al (2015)

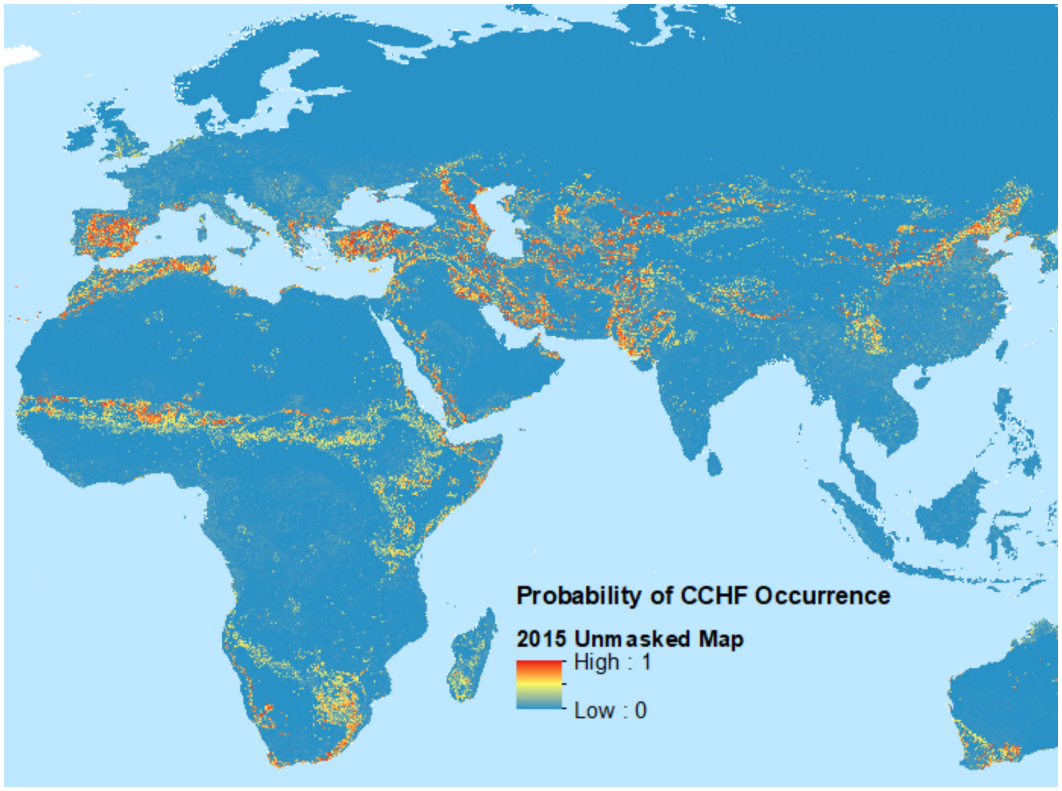

Supplementary Figure 16. Areas with > 0.75 probability of vector presence

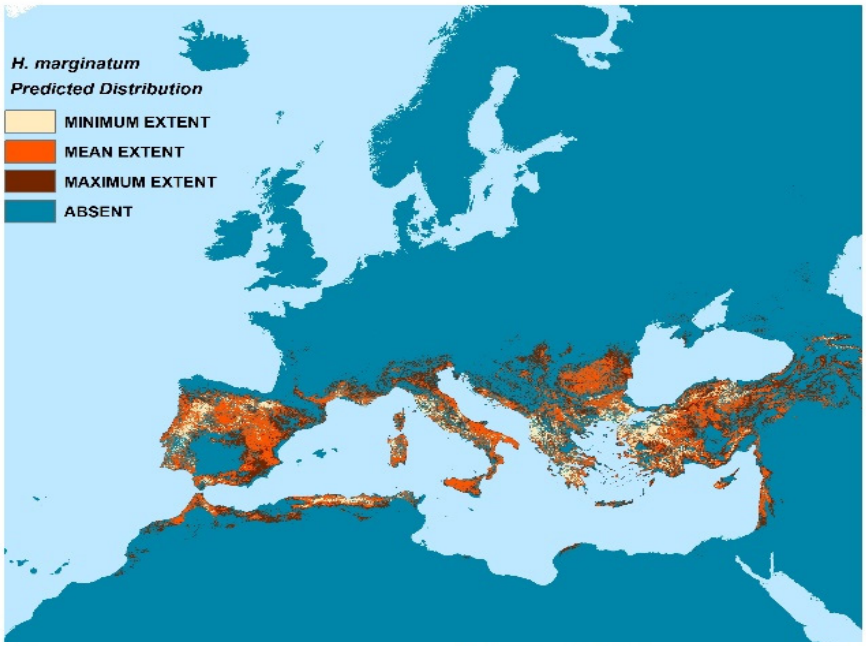

European Centre for Disease Prevention and Control (ECDC)

Gustav III:s Boulevard 40
16973 Solna, Sweden

Tel. +46 858601000
ECDC.info@ecdc.europa.eu

www.ecdc.europa.eu

Follow ECDC on social media
Twitter: @ECDC_EU
Facebook: www.facebook.com/ECDC.EU
Linkedin: www.linkedin.com/company/ecdc/

Publications Office
of the European Union